First-principles model study of the phase stabilities of dilute Fe-Cu alloys: Role of vibrational free energy

D. Reith* and R. Podloucky†

Department of Physical Chemistry, University of Vienna and Center for Computational Materials Science, Sensengasse 8, A-1090 Vienna, Austria

(Received 31 March 2009; revised manuscript received 25 May 2009; published 18 August 2009)

The aim of our first-principles study is to model dilute Fe-Cu alloys by including vibrational properties for the determination of phase boundaries. Single-atom and pairwise defects of Cu in bcc Fe and Fe in fcc Cu are considered in terms of structurally relaxed supercells, for which the corresponding total energies are calculated by a density-functional theory (DFT) approach. Based on DFT total energy differences strongly nonbonding substitutional formation energies for all defects are derived. For determining the entropy of mixing, a mechanical statistical model is designed, which is also able to include pairwise and larger defects. By the same DFT approach and within the harmonic model vibrational properties and, in particular, the temperature-dependent vibrational free energies are calculated. Based on these results a vibrational free energy for each defect species is obtained, which in combination with the corresponding DFT formation energies and the entropy of mixing is added up to a grand canonical potential. Minimizing this potential as a function of defect concentrations yields the desired free energies as a function of concentration and temperature, from which the phase boundaries are derived. Analyzing our results we find that the vibrational entropies are determining the temperature dependency of the vibrational free energies. We find, that including the vibrational free energy via the vibrational entropy is very important for explaining the rather wide miscibility range of mixing Cu to bcc Fe as observed experimentally. On the Cu-rich side of the Fe-Cu system including the vibrational entropy narrows the miscibility range.

DOI: 10.1103/PhysRevB.80.054108 PACS number(s): 81.30.Bx, 61.72.J−, 63.20.dk

I. INTRODUCTION

Fe-rich Fe-Cu alloys are of technological interest as admixtures of copper strengthen steel.[1,2] Although there is no stable intermetallic Fe-Cu compound, up to 20% copper can be added to steel, the copper inclusions being stabilized by the formation of precipitates. The phase diagram of the Fe-Cu system has a very large miscibility gap between the solid solutions at the Fe-rich and Cu-rich sides. At the Cu-rich side the range of miscibility is much narrower in comparison to the Fe-rich side.[3,4] The scientific interest focuses on the Fe-rich alloys aiming to understand the rather large miscibility range. Recent density-functional theory (DFT) calculations[5–10] as well as the present study reveal that adding Cu to an Fe matrix is energetically very unfavorable: the DFT enthalpy of formation per Cu defect is about 0.7 eV. Therefore the conclusion is that the strongly temperature-dependent miscibility of Cu in bcc Fe comes from entropy contributions to the free energy. Formation of Cu precipitations was studied by Monte Carlo approaches[9] on the basis of model potentials and fitted parameters. These techniques implicitly include the mixing or configurational entropy but its influence on the thermodynamical stability is not discussed. The influence of the vibrational free energy and the corresponding entropy, however, was not investigated so far and it is known that vibrational entropies can drive structural phase transitions, as shown, for example, in Refs. 11–13.

The main goal of the present *ab initio* study is to analyze the role of the discussed entropy terms. For this purpose, we derive temperature-dependent vibrational free energies and include them for the derivation of the thermodynamical stability of Fe-Cu solid solutions. Such a task of calculating the vibrational free energy within a truly concentration-dependent modeling of the phase stabilities (e.g., in terms of the cluster expansion[14,15]) is very demanding. Therefore, as a first step we designed a simplified model of isolated defects, namely, in terms of single and pairwise substitutes of Cu in bcc Fe and Fe in fcc Cu. For this defect model we formulated a thermodynamic model for the total free energy, in which the vibrational free energy for each defect and the entropy of mixing is contained. Thus the obtained free energy for each phase (i.e., Fe-rich and Cu-rich solid solutions) depends on temperature and concentration and is then used to derive the thermodynamical stability of each phase.

II. COMPUTATIONAL SETUP

For most of the *ab initio* calculations in our paper we used the Vienna *ab initio* simulation package (VASP) with the projector augmented wave (PAW) construction for the pseudopotential.[16–18] Test calculations for some selected cases were also done by applying the full-potential linearized augmented plane-wave method as implemented in the FLAIR code.[19,20] The exchange-correlation functional was parametrized in terms of the generalized gradient approximation (GGA) of Perdew *et al.* (PBE).[21] In some tests with the FLAIR code the GGA parametrization of Ref. 22 was also used. The PAW potential is constructed in such a way that for Fe the $3s^2$ and $3p^6$ semicore states are treated as valence states, which was also done for the $3p^6$ semicore states of Cu. For all VASP calculations an energy cutoff of 450 eV was used for the plane-wave basis set. Concerning the FLAIR calculations the cut-off energy was 280 eV. For all the calculations, apart from the test cases, unit cells of 64 atoms were

constructed. The total energies, which entered the thermodynamical quantities, were derived from calculations for which volumes and atomic positions were fully relaxed.

Supercells of 64 atoms were found to be sufficiently large for describing isolated single-atom and pairwise defects. In order to get numerically accurate formation energies the total energy calculations for the pure phases were done with the same supercell and the same set of numerical parameters.

For integration over the Brillouin zone in the VASP calculations the tetrahedron method with Blöchl's corrections[23] was used when determining the total energies, while the Methfessel-Paxton[24] smearing method with a smearing of 0.2 eV was applied for ion relaxations and for the very accurate force calculations, which are necessary for the phonon calculations. When applying FLAIR, the described smearing methods were chosen. The $\vec{k}$-point mesh for the Brillouin zone integration was generated in both the VASP and FLAIR applications by the construction of Monkhorst and Pack.[25] For the calculations involving 64 atoms supercells a $4\times4\times4$ $\vec{k}$-point mesh was chosen. The 64 atoms or $4\times4\times4$ supercell has been constructed according to the primitive vectors of the bcc and fcc lattices, accordingly.

For the calculations of the vibrational properties within the harmonic approximation the program PHON (Refs. 26 and 27) was used in combination with VASP calculations for determining the force constants. For the starting geometry (i.e., zero displacements) the atomic positions were relaxed until the forces were smaller than 10^{-4} eV/Å. The phonon density of states (PHDOS) was calculated on an $10\times10\times10$ $\vec{q}$-point mesh according to Monkhorst and Pack. Convergency of the vibrational properties, such as phonon dispersions and free energies, has been tested by comparing results for different supercells, and from that the chosen 64 atoms cell was found to be sufficiently large.

Solving numerically the set of nonlinear equations of the thermodynamical model in Sec. IV B for the concentrations c_1 and c_2, a globally convergent Newton-Raphson method[28] was used by fixing the values for the parameters μ, T and for the energies $f^{X_i}, \varepsilon^{X_i}$.

III. RESULTS AND DISCUSSION

A. Formation energies

Testing the accuracy of our calculations we compare our results with data of recent papers,[5,7] which also applied VASP within a GGA parametrization of the exchange-correlation functional. In addition, we also used the FLAIR code for some selected cases for independent cross-checks. Summarizing our tests we find that the results of our FLAIR and VASP calculations agree well with the data of Ref. 5, but are significant differences to the work of Domain *et al.*.[7] These authors used ultrasoft pseudopotentials (USPP) in contrast to the PAW potentials as chosen by Liu *et al.*[5] and by us.

Table I presents a summary of the results for the pure bcc Fe and fcc Cu phases. Concerning pure fcc Cu, all calculated data agree well with each other. For pure bcc Fe the situation is, however, different, as the results of Domain *et al.*[7] significantly differ: the lattice parameter and the total magnetic moment are larger, whereas the bulk modulus is smaller. Presumably these differences are due to the use of USPP instead of PAW potentials[18] or the all-electron full potential as utilized in FLAIR. Although the discrepancies for one Fe atom are small, errors may accumulate in supercell calculations and lead to very significant energy differences for defect energies, as discussed in the following. Applying FLAIR for Fe the two different GGA parametrizations of Refs. 22 and 21 gave the same results (see Table I), as expected for close-packed bulk systems.

TABLE I. Results of VASP and FLAIR calculations and experimental data for ground-state properties of bcc Fe and fcc Cu: cubic lattice parameter a, total magnetic moment M, and bulk modulus B for bcc Fe and fcc Cu. PAW pseudopotentials, USPP as implemented in VASP. GGA parametrizations of the exchange-correlation according to Ref. 21 (PBE) and Ref. 22 (PW91).

	Method	a (Å)	M (μ_B/at.)	B (GPa)
bcc Fe	VASP (PAW:PBE)	2.831	2.19	198
	FLAIR (PBE)	2.838	2.24	199
	FLAIR (PW91)	2.837	2.23	199
	VASP (PAW:PW91)[a]	2.827	2.16	194
	VASP (USPP:PW91)[b]	2.856	2.32	160
	Expt.[c]	2.8662	2.18	168
fcc Cu	VASP (PAW:PBE)	3.636		147
	FLAIR (PBE)	3.627		143
	VASP (PAW:PW91)[a]	3.634		134
	VASP (USPP:PW91)[b]	3.641		140
	Expt.[c]	3.614		137

[a]Reference 5.
[b]Reference 7.
[c]References 29–31.

Within a supercell approach the formation energy ε^{X_i} for a substitutional defect cluster X_i consisting of n_i defect atoms is defined by

$$\varepsilon^{X_i} = E_{\mathrm{DFT}}^{X_i+H}(n_i+n_H) - (n_H E_{\mathrm{DFT}}^{H} + n_i E_{\mathrm{DFT}}^{X_i}), \quad (1)$$

which is the difference between the total DFT energies of the supercell containing the defect cluster, $E_{\mathrm{DFT}}^{X_i+H}$, with n_i defect atoms and n_H host atoms minus the corresponding combinations of reference energies of the pure ground-state phases. (The total number of atoms in the supercell is $N=n_i+n_H$.) For Cu defects in a bcc Fe matrix the total energy for the corresponding supercell is calculated and pure fcc Cu and bcc Fe serve as reference systems. Fe defects in an fcc Cu matrix are treated in the same way.

Discussing the formation energy of one substitutional Cu defect in Fe, $\varepsilon^{\mathrm{Cu}_1}$, we compare our results with the data of Ref. 7 as collected in Table II. The table reveals a very significant difference: from all our studies we derive values for $\varepsilon^{\mathrm{Cu}_1}$ which are larger than 750 meV, whereas Domain *et al.*[7] reported values which are by at least 200 meV smaller than our results. As such a big difference will strongly alter the phase stabilities and phase diagram, we have to ensure that

TABLE II. DFT derived formation energy of one Cu defect in bcc Fe, ε^{Cu_1}, for several test cases for 16 and 64 atoms supercells. The corresponding defect energy of Fe in fcc Cu, ε^{Fe_1}, was calculated only for a 64 atoms supercell. Results are shown for no relaxation, relaxation of atomic positions, as well as relaxation of volume and positions. The number of $\vec{k}$ in the table results from multiplication of the total number of k points in the Brillouin zone times the number of atoms in the supercell. A comparison to the work of Ref. 7 is made for the 16 atoms supercell calculation of ε^{Cu_1}. Abbreviations for potentials and methods as in Table I.

	Method	Number of atoms	k points	ε no relaxation (meV)	ε atoms relaxation (meV)	ε all relaxation (meV)
Cu atoms in Fe bcc (ε^{Cu_1}):	VASP (PAW:PBE)	16	8192	768	758	
	FLAIR (PBE)	16	8192	767	756	
	VASP (USPP:PW91)	54	6750		540	500
	VASP (PAW:PBE)	64	4096	790	778	773
Fe atoms in Cu fcc (ε^{Fe_1}):	VASP (PAW:PBE)	64	1728	858	857	853

our results are correct. Therefore we performed numerous test calculations using VASP with different numerical setups as well as applying FLAIR. Table II shows results for two sizes of supercells (16 and 64 atoms) for three different cases, namely, with and without relaxation of the atomic positions, and with everything relaxed including the volume. In general the effect of relaxation on the formation energy is rather small, being less than 3%. We further tested our computational approach by recalculating some of the intermetallic Cu-Fe compounds which were needed for the cluster expansion as applied in Ref. 5, namely, FeCu (in the B2 structure), $FeCu_3$, and Fe_3Cu (both in the DO_3 structure). In all cases comparing energies and structural parameters the agreement is very good, the differences being less than 3%. Although Liu *et al.*[5] applied a GGA potential[22] different to ours[21] the results are very similar (as it was also tested for bcc Fe by FLAIR calculations, see above). Therefore using different GGA potentials (Domain *et al.* applied the one of Ref. 22) could not be the source for the discussed large differences. We rather suspect, that the usage of the USPP construction for the Fe pseudopotential in Ref. 7 is the main reason for the discrepancy.[18]

Table III lists the results of our calculations for the single and pairwise defects of Cu in bcc Fe and Fe in fcc Cu. For the pairwise defects the energy is reduced, in comparison to single defects, significantly due to the bonding between the defects but still is strongly positive. This reduction is particularly strong for Fe pairs, presumably due to their ferromagnetic coupling (antiferromagnetic coupling is less favorable by 320 meV per atom.). Anticipating the discussion about thermodynamical stability one would expect that because of the substantially lower formation energy of Fe pairs compared to the Cu pair defects, the miscibility of Fe defects in fcc Cu would be larger than the miscibility of Cu defects in bcc Fe. This is indeed the case if vibrational free energies are *not* taken into account as illustrated in Fig. 4.

TABLE III. Formation energy per atom for the single-atom, ε^{X_1}, and pairwise substitutional defects, $\varepsilon^{X_2}/2$ per atom for Cu in bcc Fe and Fe in Cu. All geometrical parameters are relaxed.

	ε^{X_1} (meV)	$\varepsilon^{X_2}/2$ (meV)	$\varepsilon^{X_2}/2-\varepsilon^{X_1}$ (meV)
Cu in Fe	773	682	−91
Fe in Cu	853	531	−322

B. Vibrational properties

Figures 1 and 2 show the differences of normalized phonon densities of states g,

$$\Delta g(\nu) = g^{X_i+H}(\nu) - g^{H}(\nu). \tag{2}$$

The results for Δg for single-atom and pairwise Cu defects in Fe are given in Fig. 1 and shows a very similar behavior for both defects. In particular, the PHDOS is significantly enhanced at lower energies between 14 and 22 meV with respect to pure Fe. This redshift might be understood by replacing Fe by heavier Cu atoms, assuming that the spring constants (i.e., bonding strength) remain rather constant. The fluctuations of Δg at larger energies are also a consequence of normalization as $\int \Delta g d\nu = 0$. The negative

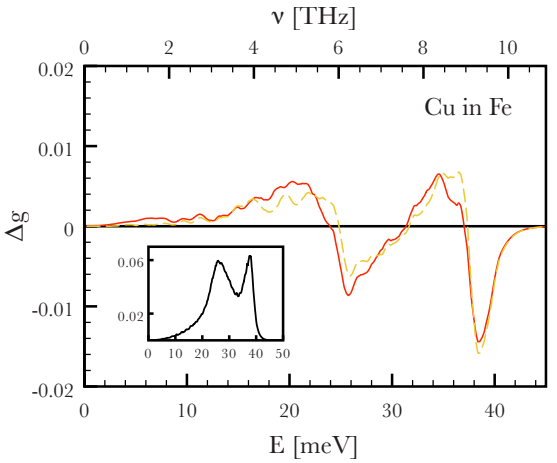

FIG. 1. (Color online) Differences Δg of normalized PHDOS for substitutional Cu defects in comparison to pure bcc Fe: single-atom Cu defect (dashed line, yellow) and pairwise Cu defect (solid line, red). The PHDOS for bcc Fe is shown in the inset.

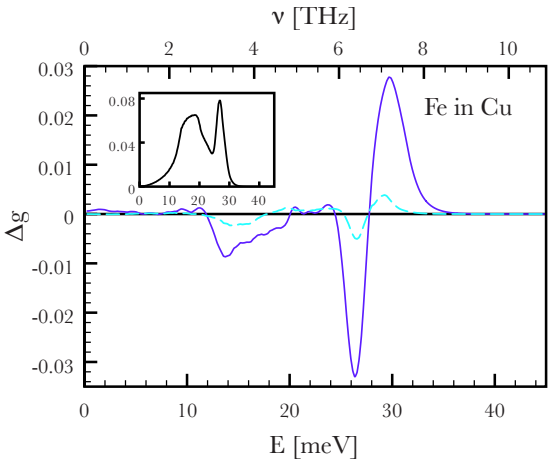

FIG. 2. (Color online) Differences Δg of normalized phonon densities of states (PHDOS) for substitutional Fe defects in comparison to pure fcc Cu: single-atom Fe defect (dashed line, turquoise) and pairwise Fe defect (solid line, blue). The PHDOS for fcc Cu is shown in the inset.

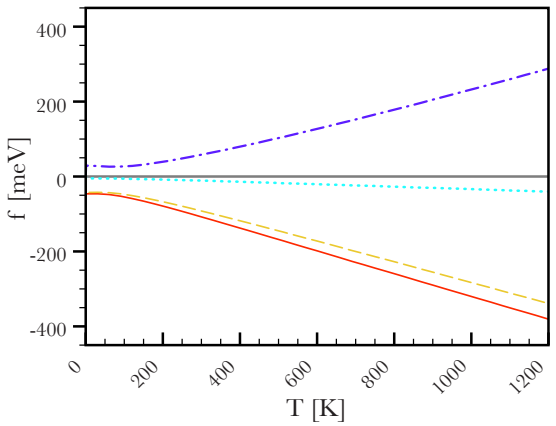

FIG. 3. (Color online) Temperature dependence of changes in differences of vibrational free energies f [see Eq. (4)]. Defects in bcc Fe: single Cu atom (dashed yellow line) and pairs of Cu atoms (solid red line); defects in fcc Cu: single Fe atom (dashed turquoise line) and pairs of ferromagnetic Fe atoms (dashed-dotted blue line). The plotted values for f_2 correspond to the vibrational defect energy for two atoms (not divided by 2).

peak centered at highest energies of about 37 meV indicates that the spectrum of defect modes is restricted to lower frequencies.

Figure 2 shows also Δg for single-atom and pairwise Fe defects in fcc Cu. The prominent features are much more pronounced for the pairwise defect, which we attribute to the strong ferromagnetic bonding between the two Fe atoms. In contrast to the Cu defects, there is a blueshift (i.e., loss of states) of the defect PHDOS at energies between 12 and 20 meV in comparison to bcc Cu. In the high-energy region above 28 meV Δg is positive, as the defect Fe atoms are lighter than the Cu host atoms. In both cases of Δg, a significant negative peak arises at medium energies centered at 25 meV, which is more pronounced with the pair wise defect.

The temperature-dependent vibrational free energy F_{phon} is derived by integration over the density of phonon states $g(\nu)$ (Ref. 32),

$$F_{phon}(T) = k_B T \int_0^\infty g(\nu) \ln\left[2 \sinh\left(\frac{h\nu}{2k_B T}\right)\right] d\nu. \qquad (3)$$

The change in the free vibrational energy $f^{X_i}(T)$ for a defect X_i substituting a host atom is expressed similarly to the DFT formation energy defined in Eq. (1),

$$f^{X_i}(T) = F_{phon}^{X_i+H}(T) - [n_i F_{phon}^{X_i}(T) + n_H F_{phon}^{H}(T)]. \qquad (4)$$

The energy $F_{phon}^{X_i+H}$ denotes the total vibrational free energy of the supercell containing n_i defect atoms and n_H host atoms. The corresponding reference pure phases, bcc Fe and fcc Cu, are the same as in Eq. (1).

Inspecting Fig. 3 and Table IV, one realizes that the temperature dependency of the defect vibrational free energies are very different for the respective defects. For Cu defects in bcc Fe (single-atom as well as pairwise defects) the behavior is very similar for both cases, namely, a strong *decrease* in f with increasing temperature, which means thermodynamical stabilization of these defects according to Eq. (11). For Fe defects in fcc Cu, however, the difference energies f behave totally different: for the single defect f is rather zero over the whole temperature range. On the other hand, for the pairwise Fe defects the vibrational free energy difference increases very strongly, which in turn reduces the thermodynamical stability of pairwise Fe defects.

Volume relaxation has a noticeable influence on $f(T)$. The energies f^{Cu_1} and f^{Cu_2} are less negative when the volume is not relaxed: for example, the difference to the volume relaxed defects at 1200 K is ≈240 meV, and for $T=800$ K it is ≈160 meV. This effect can also be observed on the Cu-rich side, where $f^{\mathrm{Fe}1}$ and $f^{\mathrm{Fe}2}$ are by about 30 meV less negative at 800 K and $f^{\mathrm{Fe}1}$ is by 40 meV less negative at 1200 K while it is 130 meV less for $f^{\mathrm{Fe}2}$.

It should be noted, that for all the studied cases the temperature dependence of f comes exclusively from the differences of vibrational entropies. The corresponding differences of internal energies are rather independent of temperature (at least on the energy scale of Fig. 3).

All values of $f(T)$ have been calculated at the equilibrium lattice constants at $T=0$ K for each of the defects. Effects of

TABLE IV. Temperature dependence of the differences of vibrational free energy, f^{X_1} and $f^{X_2}/2$, according to Eq. (4).

	T (K)	f_1 (meV)	$f_2/2$ (meV)
Cu in Fe:	0	−43	−23
	400	−118	−69
	800	−227	−130
	1200	−339	−191
Fe in Cu:	0	−5	29
	400	−14	80
	800	−28	178
	1200	−40	288

thermal expansion were not taken into account, because we assume that the *differences* of free energies $f(T)$ are only weakly affected by the thermal expansion. However, *total* vibrational free energies might be strongly influenced by thermal expansion, as shown, for example, in Ref. 33.

IV. THERMODYNAMICAL APPROACH

The grand canonical approach of Refs. 34 and 35 for single-atom pointlike defects within a supercell approach is extended to include also pairs of defect atoms and to take into account the vibrational free energy of the defects.

A. Configurational entropy

In the spirit of Kikuchi *et al.*[36] the configurational entropy is defined in terms of bonds, which allows the inclusion of pairwise or higher-order substitutional defects. The basic perception is that the distribution of a particular substitutional defect cluster X_m is given by

$$W_m(B_m,b_m) = \binom{B_m}{b_m}, \tag{5}$$

in which B_m denotes the total number of available bonds in the system for the defect cluster X_m and b_m is the actual number of bonds occupied by n_m defect clusters X_m. The resulting distribution for a set of independent defect clusters $X_1 \ldots X_n$ occurring $n_1 \ldots n_m$ times in the system will then be a product of the corresponding distributions $W_1 \ldots W_m$. The configurational entropy S_{config} as derived from these distributions has to be finally divided by the total number of available bonds, making S_{config} independent of the actual size of the system. For the present purpose S_{config} has to be evaluated for a mixture of n_1 single-atom defects X_1 and n_2 pairwise atom defects X_2.

Each lattice site is connected to its neighboring sites by ω bonds, whereby ω is half of the number of nearest-neighbor distances for a given lattice. For example, the numbers $\omega = 4$ or 6 correspond to a bcc or fcc lattice, respectively. The total number of bonds B for a given lattice with N lattice sites is consequently defined as $B = \omega N$. The n_1 single-atom defects are connected by $b_1 = \omega n_1$ bonds to the remaining sites. If no other defects are present the distribution of all such single defects amounts to

$$W_1(B_1,b_1), \quad B_1 = B, \quad b_1 = \omega n_1 \tag{6}$$

and the resulting entropy S_{config}, after it was divided by B, will be the standard entropy for a regular solution.

Considering pairwise substitutional defects their distribution now depends on their neighborhood. A substitutional pairwise defect contains one complete bond, namely, the bond which connects the two defect atoms forming the defect. Therefore, for n_2 such defects the total number of available number of bonds is now $B_2 = B - n_2$, and the number of different distributions of these defects amounts to

$$W_2(B_2,b_2), \quad B_2 = B - n_2, \quad b_2 = (2\omega - 1)n_2 \tag{7}$$

as each pairwise defect is connected by $2\omega - 1$ bonds to the neighboring sites.

The resulting total number of distributions W_{1+2} of single and pairwise defects is described by the product of distributions of single and pairwise defects by

$$W_{1+2} = W_2(B_2,b_2)W_1(B_2 - b2,b_1) \tag{8}$$

$$= \frac{B_2!}{b_1!\, b_2!\, (B_2 - b_1 - b_2)!}. \tag{9}$$

It should be noted, that the number of available bonds for the single defects is now reduced to $B - 2\omega n_2$, because $2n_2$ sites are occupied by atoms belonging to the pairwise defects. Making use of Eq. (7) this difference is equal to $B2 - b2$.

Applying Stirling's approximation and dividing by $B = \omega N$, the configurational entropy for a mixture of independent single and pairwise substitutional defects finally amounts to

$$S_{conf} = k_B \left[\left(1 - \frac{c_2}{\omega}\right) \ln\left(\frac{1 - \frac{c_2}{\omega}}{1 - c_1 - 2c_2} \right) - \kappa c_2 \ln\left(\frac{\kappa c_2}{1 - c_1 - 2c_2} \right) - c_1 \ln\left(\frac{c_1}{1 - c_1 - 2c_2} \right) \right], \tag{10}$$

in which the abbreviation $\kappa = \frac{2\omega - 1}{\omega}$ and the concentrations $c_1 = n_1/N$, $c_2 = n_2/N$ of the single and pairwise defects are introduced. If the number of pairwise defects is zero, i.e., $c_2 = 0$ then the well-known expression of S_{config} for a regular solution is rederived.

B. Grand canonical approach

In our case, the total free energy F_{tot} consists of the sum of the single and pairwise defects formation and vibrational energies (see Secs. III A and III B) and the configurational entropy,

$$F_{tot}(c1,c2,T) = -TS_{conf}(c1,c2) + [\varepsilon^{X_1} + f^{X_1}(T)]c_1 + [\varepsilon^{X_2} + f^{X_2}(T)]c_2 \tag{11}$$

at zero pressure. (It should be noted, that the vibrational entropies per defect are included in the free energies f_i^X.) The total number of defect atoms amounts to $N^X = n_1 + 2n_2$. The factor 2 occurs, because each pairwise defect consists of two atoms. As mentioned, entropy terms due to changes in magnetic order (i.e., the transition from ferromagnetic ordering to a paramagnetic state) are not included but might be taken into account by adding a suitable entropy term to F_{tot}.

Consequently, the total number of remaining host atoms is the difference $N^H = N - N^X$ with respect to the total number of all atoms N in the system. A generalized grand canonical potential J' (Refs. 34 and 35) obeying the constraint $N^X = n_1 + 2n_2$ can now be constructed introducing the Lagrangian parameter μ as the chemical potential of the system and making use of the concentrations $x = N^X/N$, $c_i = n_i/N$,

$$J'(c_1,c_2) = F_{tot} + \mu(x - c_1 - 2c_2). \tag{12}$$

Minimizing the potential J' with respect to the concentrations c_1, c_2 results in the set of nonlinear equations,

$$e^{-\beta(f^{X_1}+\varepsilon^{X_1}-\mu)} = \frac{c_1}{1-c_1-2c_2}, \tag{13}$$

$$e^{-(\beta/2)(f^{X_2}+\varepsilon^{X_2}-2\mu)} = \frac{\left(1-\frac{c_2}{\omega}\right)^{1/2}(\kappa c_2)^{\kappa/2}}{1-c_1-2c_2}, \tag{14}$$

in which the abbreviation $\beta=(k_BT)^{-1}$ was applied. The set of equations of Eqs. (13) and (14) now have to be solved numerically. For the Fe-Cu alloy system the concentrations c_1, c_2 were calculated for the Fe-rich side (Cu single and pairwise substitutional defects in bcc Fe) as well as for the Cu-rich side (Fe single and pairwise substitutional defects in fcc Cu) and the corresponding free energies F_{tot} were calculated for both ends of the phase diagram. The thermodynamical stable boundaries in the T,x phase diagram were calculated by the standard common tangent procedure connecting the corresponding (negative) potentials J' at the Cu-rich and Fe-rich sides for a fixed temperature T. The corresponding metastable boundaries were determined by searching for the values of T,x at which the potential J' became positive.

C. Phase diagram

Figure 4 shows the phase diagram for the dilute Fe-Cu alloy system at the Fe-rich and Cu-rich sides. No other stable phases exist over the whole range of concentrations, as it is clearly evidenced by the rather large and positive (i.e., nonbonding) formation energies derived from DFT calculations for Fe-Cu ordered compounds.[5] Therefore, only solid solutions and precipitations might be thermodynamically stabilized by entropy.

In Fig. 4(a) for the Fe-rich alloy experimental data[4] (dash-dotted line) and empirical calculation of phase diagram (CALPHAD) modeling[3] (dotted line) indicate that a significant amount of Cu can be added. Our results are in good agreement with both the CALPHAD model and experimental boundaries, as both lie within the hatched region. It should, however, be noted that our model only covers single and pairwise defects. Larger Cu clusters might lead to even more favorable lower boundaries, if there is a sufficient gain in bonding energy for larger clusters compared to pairs of Cu atoms. On the other hand, considering Fig. 4(b) and comparing the yellow and red lines, there is almost no change in the phase boundary when pairwise defects are added to the mixture with single-atom Cu defects.

The situation is very different at the Cu-rich side, where the miscibility range is rather narrow, as indicated by the (rather inaccurate) experimental boundary.[4]

From our calculated results in Fig. 4(b) *without* vibrational free energies, we derive a very narrow miscibility range at the Fe-rich side (colored dashed lines), and a wider range at the Cu-rich side (dashed blue line). The mixing entropy alone is obviously totally insufficient for a reasonable estimate of the phase boundaries. Including now vibrational free energies changes the calculated results dramatically. Figure 4(b) emphasizes this findings, for the Fe-rich side by looking at the dashed and solid lines: the miscibility range widens significantly whereas at the Cu-rich side it is strongly narrowed. This asymmetric behavior of the miscibility ranges is due to the asymmetry of the total free energies F_{tot} of both phases: whereas at the Fe-rich side the vibrational energy (i.e., the vibrational entropy) lowers F_{tot}, the effect is opposite on the Cu-rich side, as illustrated in Fig. 3.

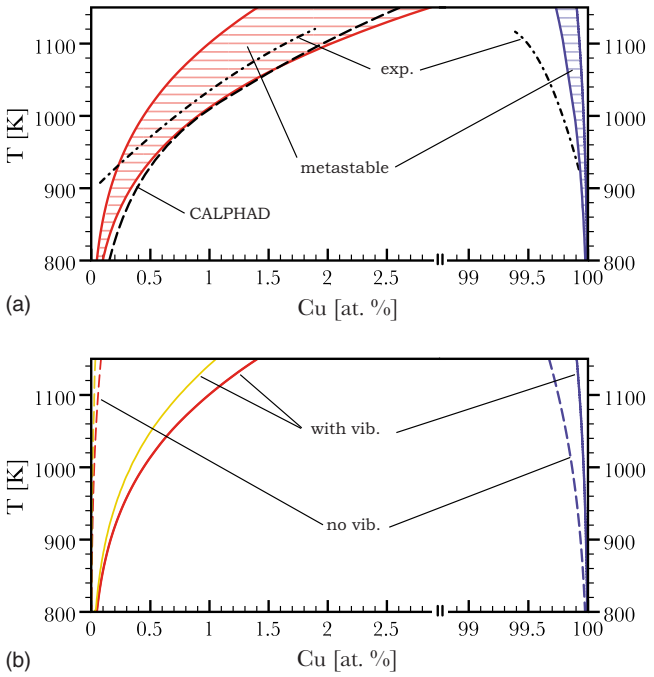

FIG. 4. (Color online) Phase diagram of the Fe-Cu system at the Fe-rich and Cu-rich sides. Panel (a): Comparison between empirical CALPHAD calculations (Ref. 3) (black dashed line) and the experimental data of Ref. 4 (black dash-dotted lines) to our calculations including the vibrational energy according to Eq. (11). Hatched areas: regions of metastable phases. The upper boundaries of the hatched areas mark the thermodynamically stable phase boundaries. Panel (b): analysis of our calculated results for the thermodynamically stable phase boundaries. Without vibrational energies: dashed lines, with vibrational energies: full lines. Results for single and both (single and pairwise) defects at the Fe-rich side are shown in yellow and red colors, correspondingly. On the Cu-rich side only the results for both (or rather pairwise) defects are shown (blue color), because the effect of single defects is hardly visible.

For a truly quantitative description of the phase boundary on the Fe-rich side for temperatures $T>T_C=1043$ K larger than the Curie temperature of Fe, the change in magnetic ordering needs also to be included. Modeling temperature-dependent magnetism is very complicated and is far beyond the scope of our work. Nevertheless, the most important effects occur already rather far below T_C (see Fig. 4), namely, that vibrational entropy has to be included for the modeling of the Fe-Cu alloys. This is also manifested by Table V. For the Fe-rich side it shows, that *without* vibrational energies the Cu concentrations c_1 and $2c_2$ are rather equal, at least in the given temperature range of 800 K$<T<$1200 K. This balance changes dramatically when vibrational entropies are included, as single-atom defects are much more abundant

TABLE V. Relative distribution of one atom and pairwise defects (in % of x) at 800 and 1200 K, and the corresponding total concentration x of the solute species.

		Without vibration			With vibration		
	T (K)	x (at. %)	c_1	$2c_2$	x (at. %)	c_1	$2c_2$
Cu in Fe	800	0.003	49	51	0.047	75	25
	1200	0.115	48	52	1.940	75	25
Fe in Cu	800	0.024	2	98	0.006	9	91
	1200	0.419	6	94	0.124	30	70

than pairs, the ratio is now 3 to 1. In both cases the mixture of defects remains rather constant in the studied temperature range. At the Cu-rich side the mixture of defects for the calculation *with* vibrational energies depends much stronger on temperature: for 800 K the ratio $c_1:2c_2$ is 1:10, and it changes to 3:7 at 1200 K. Clearly, the magnetic coupling of the Fe pairs manifests itself in the dominance of the pairwise defects.

V. SUMMARY

By first-principles density-functional supercell calculations and thermodynamical modeling for dilute Fe-Cu alloys we demonstrated that vibrational free energies may have a substantial influence on the thermodynamical stability and miscibility range of solid solutions in particular. The Fe-Cu alloy system is very well suited for such a task, as the rather wide miscibility range at the Fe-rich side can only be produced by entropic effects: no stable intermetallic phase exists and the formation energies of Cu and Fe defects as derived from density-functional calculations are highly positive and nonbonding. Modeling dilute alloys we considered single-atoms and pairwise substitutional defects, for which we formulated a suitable entropy of mixing. This formulation can be extended to any size and mixtures of isolated defects. Applying a density-functional theory approach for the first-principles determination of vibrational properties within the harmonic approximation we derived temperature-dependent free vibrational energies for each defect species, which were implemented in a grand canonical formulation of the total free energy. Magnetic interactions were included in terms of spin-polarized calculations, but the change in magnetic ordering at the Curie temperature of Fe is not taken into account.

The major finding of our work is that indeed the vibrational free energies (in particular their entropy contributions) are very important, and by including them we could reproduce the main features of the experimentally estimated phase diagram at low concentrations, namely, the wide miscibility range at the Fe-rich side and the very narrow range at the Cu-rich side. It would be highly desirable to extend the spirit of our study to a concentration-dependent modeling of phase stabilities. In particular the formation of precipitation may be strongly influenced by taking into account the effect of vibrational energies. We propose to perform such a task in terms of the cluster expansion[14,15] for which temperature-dependent cluster interaction energies need to be derived. For that it would be necessary to calculate vibrational energies for each structure, which enters the cluster expansion: an extensive but feasible task.

ACKNOWLEDGMENT

This work was supported by the Austrian science fund FWF under Grant No. P18480-N19.

*david.reith@univie.ac.at
†raimund.podloucky@univie.ac.at

[1] S. Lahiri and M. Fine, Metall. Trans. B **1B**, 1495 (1970).
[2] M. Fine and D. Isheim, Scr. Mater. **53**, 115 (2005).
[3] M. Turchanin, P. Agraval, and I. Nikolaenko, J. Phase Equilib. **24**, 307 (2003).
[4] B. Predel, *Phase Equilibria, Crystallographic and Thermodynamic Data of Binary Alloys*, edited by O. Madelung, Landolt-Börnstein, New Series, Group IV, Vol. 5, Pt. D (Springer-Verlag, Berlin, 1994).
[5] J. Z. Liu, A. van de Walle, G. Ghosh, and M. Asta, Phys. Rev. B **72**, 144109 (2005).
[6] M. E. Fine, J. Z. Liu, and M. D. Asta, Mater. Sci. Eng., A **463**, 271 (2007).
[7] C. Domain and C. S. Becquart, Phys. Rev. B **65**, 024103 (2001).
[8] C. Becquart and C. Domain, Nucl. Instrum. Methods Phys. Res. B **202**, 44 (2003).
[9] E. Vincent, C. S. Becquart, C. Pareige, P. Pareige, and C. Domain, J. Nucl. Mater. **373**, 387 (2008).
[10] K. Yuge, A. Seko, I. Tanaka, and S. R. Nishitani, Phys. Rev. B **72**, 174201 (2005).
[11] C. Colinet, W. Wolf, R. Podloucky, and A. Pasturel, Appl. Phys. Lett. **87**, 041910 (2005).
[12] X.-Q. Chen, W. Wolf, R. Podloucky, and P. Rogl, Phys. Rev. B **76**, 014424 (2007).
[13] X.-Q. Chen, W. Wolf, R. Podloucky, and P. Rogl, Phys. Rev. B **76**, 092102 (2007).
[14] J. Sanchez, F. Ducastelle, and D. Gratias, Physica A **128**, 334 (1984).
[15] S. Müller, J. Phys.: Condens. Matter **15**, R1429 (2003).
[16] P. E. Blöchl, Phys. Rev. B **50**, 17953 (1994).
[17] G. Kresse and J. Furthmüller, Phys. Rev. B **54**, 11169 (1996).
[18] G. Kresse and D. Joubert, Phys. Rev. B **59**, 1758 (1999).
[19] M. Weinert, E. Wimmer, and A. J. Freeman, Phys. Rev. B **26**, 4571 (1982).
[20] M. Weinert, G. Schneider, R. Podloucky, and J. Redinger, J. Phys.: Condens. Matter **21**, 084201 (2009).
[21] J. P. Perdew, K. Burke, and M. Ernzerhof, Phys. Rev. Lett. **77**, 3865 (1996).
[22] J. P. Perdew, J. A. Chevary, S. H. Vosko, K. A. Jackson, M. R.

Pederson, D. J. Singh, and C. Fiolhais, Phys. Rev. B **46**, 6671 (1992).
[23] P. E. Blöchl, O. Jepsen, and O. K. Andersen, Phys. Rev. B **49**, 16223 (1994).
[24] M. Methfessel and A. T. Paxton, Phys. Rev. B **40**, 3616 (1989).
[25] H. Monkhorst and J. Pack, Phys. Rev. B **13**, 5188 (1976).
[26] D. Alfè, 1998, the program is available at http://chianti.geol.ucl.ac.uk/~dario
[27] D. Alfè, G. D. Price, and M. J. Gillan, Phys. Rev. B **64**, 045123 (2001).
[28] W. H. Press, B. P. Flannery, S. A. Teukolsky, and W. T. Vetterling, *Numerical Recipes: The Art of Scientific Computing* (Cambridge University Press, Cambridge, 2007), pp. 473–477.
[29] M. Stearns, *Magnetic Properties of Metals*, edited by H. P. J. Wijn, Landolt-Börnstein, New Series, Group III, Vol. 19, Pt. A (Springer-Verlag, Berlin, 1994).
[30] P. Eckerlin and H. Kandler, *Structure Data of Elements and Intermetallic Phases*, edited by K.-H. Hellwege and A. M. Hellwege, Landolt-Börnstein, New Series, Group III, Vol. 6 (Springer-Verlag, Berlin, 1994).
[31] A. G. Every and A. K. McCurdy, *High and Low Frequency Properties of Dielectric Crystals: Second and Higher Order Elastic Constants*, edited by D. F. Nelson, Landolt-Börnstein, New Series, Group III, Vol. 29, Pt. A (Springer-Verlag, Berlin, 1994).
[32] S. Müller, W. Wolf, and R. Podloucky, *Alloy Physics*, edited by W. Pfeiler (Wiley-VCH, Weinheim, 2007), Chap. 11, p. 605.
[33] W. Frank, U. Breier, C. Elsässer, and M. Fähnle, Phys. Rev. Lett. **77**, 518 (1996).
[34] J. Mayer and M. Fähnle, Acta Mater. **45**, 2207 (1997).
[35] B. Meyer and M. Fähnle, Phys. Rev. B **59**, 6072 (1999).
[36] R. Kikuchi, Phys. Rev. **81**, 988 (1951).